water

MDPI

Article

Impact of Inorganic Mineral Release on Groundwater System During Oil Shale In-Situ Exploitation

Qingyu Li [1,2], Laijun Lu [1], Quansheng Zhao [2] and Shuya Hu [2,*]

[1] College of Earth Sciences, Jilin University, Changchun 130021, China
[2] College of Environmental Science and Engineering, Qingdao University, Qingdao 266071, China
* Correspondence: 90shuya@qdu.edu.cn

Abstract: The release of inorganic minerals from oil shale, oil shale ash and surrounding rock to groundwater during in-situ mining were discussed. The results showed that both ambient temperature and reaction time affected the release of anions and cations. Ca^{2+} is the main cation in aqueous solution at 20 °C and 50 °C, and Na^{+} is the main cation in aqueous solution at 80 °C and 100 °C. HCO_3^- is the main anion in the aqueous solution under different reaction conditions. With increasing temperature and the progress of the reaction, the content of Ca^{2+}, Mg^{2+}, and HCO_3^- decreased (which is different from other ions) and the water chemical types in the three aqueous solutions change. The hydrochemical type of oil shale ash-aqueous solution is SO_4·HCO_3-Na+K at 80 °C and 100 °C, which is converted to sulfuric acid and changes the water quality. The results show that the release of inorganic minerals from oil shale to groundwater due to the heat released during the in-situ exploitation of oil shale cannot be ignored.

Keywords: oil shale in-situ exploitation; groundwater; water-rock interaction; inorganic minerals; hydrogeochemistry

Citation: Li, Q.; Lu, L.; Zhao, Q.; Hu, S. Impact of Inorganic Mineral Release on Groundwater System During Oil Shale In-Situ Exploitation. *Water* **2022**, *14*, x. https://doi.org/10.3390/xxxxx

Academic Editor(s):

Received: date
Accepted: date
Published: date

Publisher's Note: MDPI stays neutral with regard to jurisdictional claims in published maps and institutional affiliations.

Copyright: © 2022 by the authors. Submitted for possible open access publication under the terms and conditions of the Creative Commons Attribution (CC BY) license (https://creativecommons.org/licenses/by/4.0/).

1. Introduction

The reserves of oil on Earth are well known to be limited. And the oil shale has become one of our research foci duo to its huge reserves (four times than the world's proven conventional oil reserves)[1-6]. But because oil shale is often interbedded with coal and carbonaceous mudstone, the exploitation of oil shale becomes very difficult, and environmental pollution is one of the difficulties[7-10].To reduce the damage to the environment caused by exploitation, scientists around the world have put forward a variety of methods for the in-situ exploitation of oil shale[11-14]. Compared with traditional surface retorting technology, in situ exploitation does not require mining, transportation or ore processing, but instead heat is directly supplied by thermal conduction or thermal radiation to the underground oil shale layer so that the oil shale is cracked underground to generate oil and gas, and then the pyrolysis oil and gas are recovered[15-19].

Under natural conditions, the oil shale layer and upper surrounding rock usually form a dense waterproof layer. However, a large amount of pyrolytic water will be produced during the in situ exploitation of oil shale. In the process of mining, the rock mass ruptures into cracks with increasing thermal stress resulting in the release of organic matter[20]. Fracturing and pyrolysis will change the original stress of the overlying rock mass. When the stress exceeds the shear strength of the rock, the rock layer will fracture, resulting in a series of water-conducting fracture zones. The in-situ pyrolysis process causes the oil shale layer to gradually change from the previously water-tight layer or weakly permeable layer to a permeable layer[21-23]. This evolution may lead to a hydraulic connection between the oil shale mining layer and the surrounding aquifer, resulting in different degrees of water-rock interaction between groundwater and oil shale, the ash and slag of oil shale after mining, and the surrounding oil shale rocks[24].

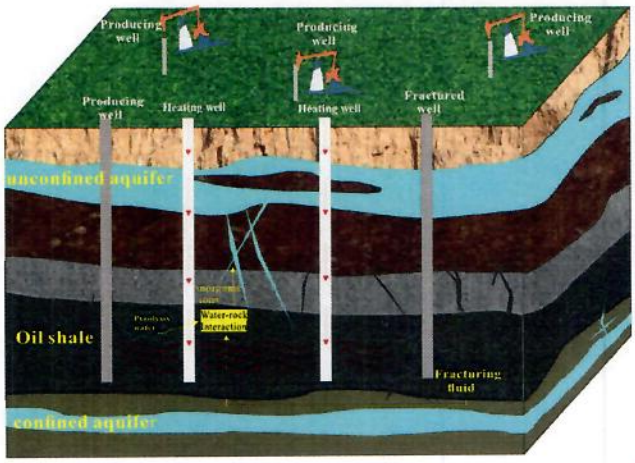


Figure 1. Conceptual model for oil shale in-situ exploitation.

Regarding the effect of in situ pyrolysis of oil shale on groundwater, a few studies have considered the potential pollution risk of water-rock interaction solutions in oil shale to groundwater, and a series of experimental studies has been carried out. Amy analyzed the organic components leached from in situ pyrolysis waste oil shale by conducting a series of continuous indoor over column leaching experiments, which determined that organic contaminants in the leachate would seriously degrade the groundwater quality within the mining area, and it would take decades for the water quality to recover[25]. Wang performed ultrapure water-rock interaction experiments. The results showed that Pb tended to accumulate in solid residues during pyrolysis. The influence of solid residue after pyrolysis of oil shale on the groundwater environment is a continuous process[26]. Hu conducted a series of water-rock interaction experiments between oil shale-water and oil shale ash-water to study the release of organic matter from groundwater during oil shale in situ exploitation. The results showed that the formation of fracture zones promoted by pyrolysis of oil shale will cause organic contaminants to diffuse into deeper groundwater and affect the quality of groundwater[21]. Related studies mainly discuss the impact of organic pollution and heavy metals on the groundwater environment during in situ oil shale mining[27-29], but few of the previous reports have focused on the impact of inorganic mineral components in the groundwater environment. However, the in-situ exploitation of oil shale is a long process accompanied by heating; for example, the in-situ conversion process (ICP) utilizes electricity to heat the oil shale underground needs to continue over 2 years[23]. Studies have shown that oil shale exploitation affects the formation temperature field for a long time, approximately four times the heating time[21,23]. Therefore, under long-term hydrothermal conditions, the release of inorganic minerals from oil shale to the groundwater environment should not be ignored.

In this study, a series of water-rock interaction experiments including oil shale and water, oil shale ash and water, and surrounding rock and water was conducted. We try to identify the mineral elements of oil shale, oil shale ash, or surrounding rock released into groundwater during the simulated in-situ mining process and analyze the potential impact of in situ recovery of oil shale on the aquifer system.

2. Materials and Methods

2.1. Study Area and Samples

The samples were collected from the Nong'an oil shale ore-bearing area, which belongs to the western edge of the northeast uplift belt of the Songliao Basin (Figure 2). This area is a stable geological environment with stable crust and relatively minimal tectonic activity. The oil yield is generally 3.5-5%.

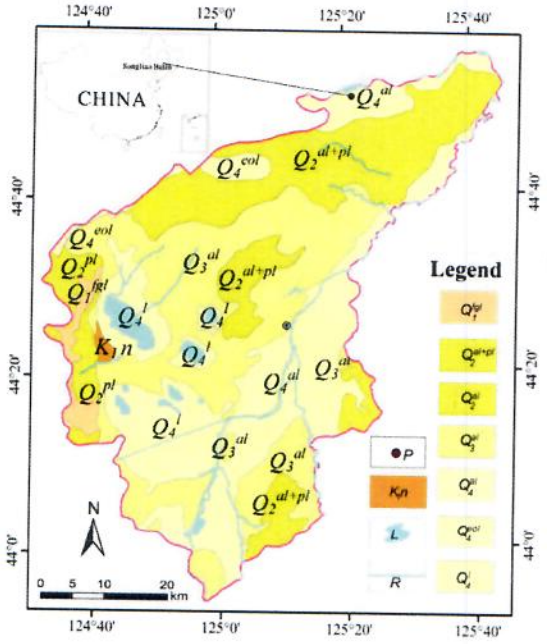


Figure 2. Geological map of Nong'an city[24]. ($Q1^{fgl}$ represents the glaciofluvial accumulation layer of Gelasian Quaternary Pleistocene, Q_2^{al+pl} represents the alluvium and diluvium of Middle Quaternary Pleistocene, Q_2^{al} represents the alluvium of Middle Quaternary Pleistocene, Q_3^{al} represents the alluvium of Upper Quaternary Pleistocene, Q_4^{al} represents the alluvium of Quaternary Holocene, Q_4^{eol} Represents the eolian deposit of Quaternary Holocene, Q^{l}_4 represents the lake sediments of Quaternary Holocene, K_{1n} represents the mudstone or clastic rock of Lower Cretaceous. In addition, L represents the lakes, R represents the rivers, and P represents the sampling site of the oil shale in the area.).

The stratified oil shale blocks and surrounding rock of the upper layer of oil shale were sealed and brought back to the lab, crushed and screened to a size range of 2-3 cm to obtain experimental samples. The oil shale and surrounding rock were dried in an oven at 110 °C for 4 hours before weighing. Some of the samples of oil shale and the surrounding rock were further ground following XRD sample preparation requirements and subjected to XRD analysis to identify minerals and other crystalline phases in the samples.

2.2. *Experiment of Water-rock Interaction*

Oil shale was heated to 400 °C in a tube furnace under nitrogen for 1h to obtain oil shale ash samples. Nitrogen is introduced to maintain an oxygen-free environment, since oil shale can only be pyrolysed under anaerobic conditions. Ultrapure water (1L) was added to 100 g oil shale, oil shale ash, and surrounding rock samples. The samples were placed in water baths with separation temperatures of 20±0.1 °C, 50±0.1 °C, 80±0.1 °C, and 100±0.1 °C. Each temperature tank had 10 samples, and they are independent of each other. Samples were soaked for 0.5, 1, 2, 5, 8, 15, 20 and 30 days. After soaking, the aqueous solution sample was filtered and tested.

2.3. *Cation content determination*

The calcium content in the solution was determined by ethylenediaminetetraacetic acid (EDTA) ($C_{10}H_{14}N_2O_8Na_2 \cdot 2H_2O$) titration. The contents of K^+, Na^+, and Mg^{2+} were measured by a Shimadzu AA-6000CF atomic absorption spectrophotometer.

2.3. Anion content determination

The content of carbonate and bicarbonate ions in the solution was measured by the acid standard solution titration method (national standard method DZ/T 0064.49 -2021). The content of F^-, Cl^-, NO_3^- and SO_4^{2-} in aqueous solution were determined by a Vantone 861 double inhibitory ion chromatograph.

3. Results

3.1. Mineral composition of samples

XRD analysis of oil shale from the Nong'an Formation reveals a complex mineral signature (Figure 3). The dominant mineral phases of oil shale and the surrounding rock in Nong'an are roughly the same, and the main minerals are plagioclase ($Na[AlSi_3O_8]$-$Ca[Al_2Si_2O_8]$), illite ($KAl_2[(SiAl)_4O_{10}]\cdot(OH)_2\cdot nH_2O$), pyrite ($FeS_2$), calcite ($CaCO_3$), dolomite ($CaMg(CO_3)_2$), zeolite ($A_mB_pO_{2p}\cdot nH2O$), quartz ($SiO_2$) and montmorillonite ($(Na,Ca)_{0.33}(Al,Mg)_2[Si_4O_{10}](OH)_2\cdot nH_2O$). However, the contents of different minerals in oil shale and the surrounding rock are obviously different. For example, the content of pyrite (FeS_2) in oil shale is higher than that in the surrounding rock, while the content of dolomite ($CaMg(CO_3)_2$) in the surrounding rock is higher than that in oil shale. In addition, there are zeolite ($A_mB_pO_{2p}\cdot nH_2O$) and montmorillonite ($(Na,Ca)_{0.33}(Al,Mg)_2[Si_4O_{10}](OH)_2\cdot nH_2O$) in the surrounding rock, which are not detected in the oil shale samples.

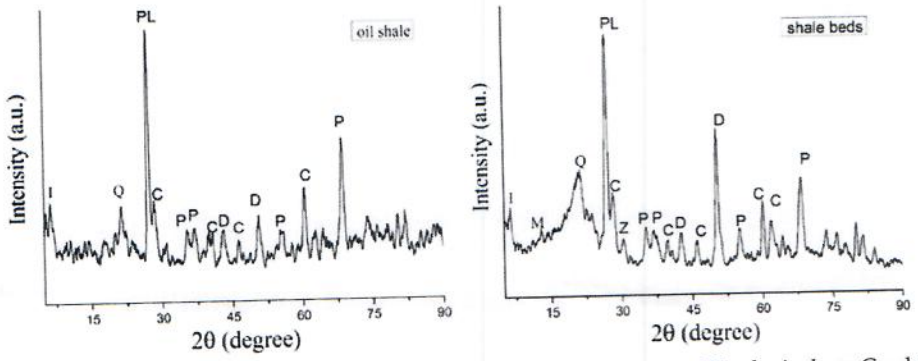


Figure 3. XRD-spectrums of oil shale and shale beds. I-illite; Q-quartz; PL-plagioclase; C-calcite; P-pyrite; D-dolomite; M-montmorillonite; Z-zeolite.

3.2. Main cation variation characteristics

Figure 4 shows the changes in the main cation content in oil shale-water solutions at different reaction temperatures. There is little difference in the contents of the four cations in the aqueous solution under the reaction conditions of 20 °C and 50 °C. At reaction temperatures of 20 °C and 50 °C, the content of Ca^{2+} is the highest, followed by K^+ and Na^+, and the content of Mg^{2+} is the lowest. At reaction temperatures of 80°C and 100 °C, the content of Na^+ in the oil shale-water solution changes strongly; the Na^+ content is the highest, followed by K^+ and Ca^{2+}, and the Mg^{2+} content is the lowest, possibly because Ca^{2+} and Mg^{2+} in aqueous solution come mainly from the dissolution of dolomite ($CaMg(CO_3)_2$) and calcite ($CaCO_3$). With increasing temperature, the solubility of dolomite ($CaMg(CO_3)_2$) and calcite ($CaCO_3$) decreases.

Moreover, K^+ changes little at 20 °C, 50 °C, and 80 °C but increases rapidly at 100 °C, indicating that a temperature of approximately 100 °C has the greatest influence on the K^+ content. The cation content in the aqueous solution tends to be stable at approximately 15 days.

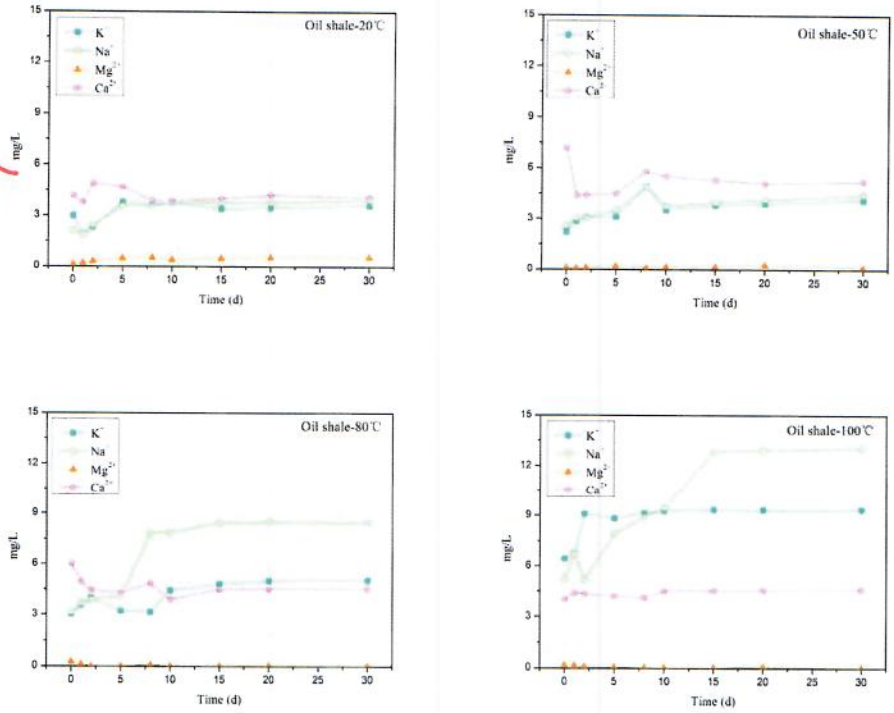


Figure 4. Variations in the content of the main cations in oil shale-aqueous solution under different temperature reaction conditions.

As shown in Figure 5, compared with the cation content in the oil shale-aqueous solution, the cation content in the oil shale ash-aqueous solution shows a different trend with increasing reaction temperature. Under different reaction temperatures, the K^+ content in oil shale ash-aqueous solution always remains the highest, and the K^+ content at 50 °C, 80 °C, and 100 °C is twice the K^+ content at 20 °C. At 20 °C, the average content of Na^+ (5.79 mg/L) was lower than the average content of Ca^{2+} (7.10 mg/L), but with increasing reaction temperature, the Na^+ content gradually increased and remained higher than the Ca^{2+} content. Ca^{2+} has a declining trend with increasing temperature. Under a reaction temperature of 100 °C, the Na^+ content in the oil shale ash-aqueous solution increases rapidly with increasing reaction time. After 30 days of reaction, the average contents of Na^+ and K^+ in the oil shale ash-aqueous solution are higher than those in oil shale-aqueous solution. This may be because high-temperature pyrolysis (>350 °C) precipitates organic matter in oil shale, increases the pore space of oil shale, and thus increases the specific surface area of oil shale ash for the reaction with the aqueous solution. On the other hand, high-temperature pyrolysis (>350 °C) will also break the structure of inorganic minerals and cause clay minerals to dewater, thus forming more pores[31].

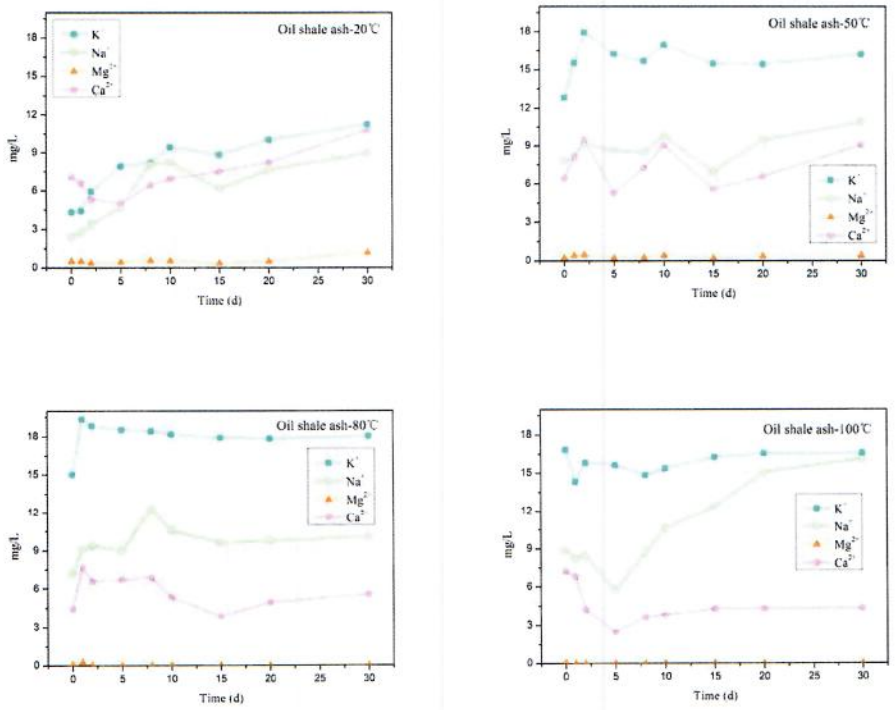
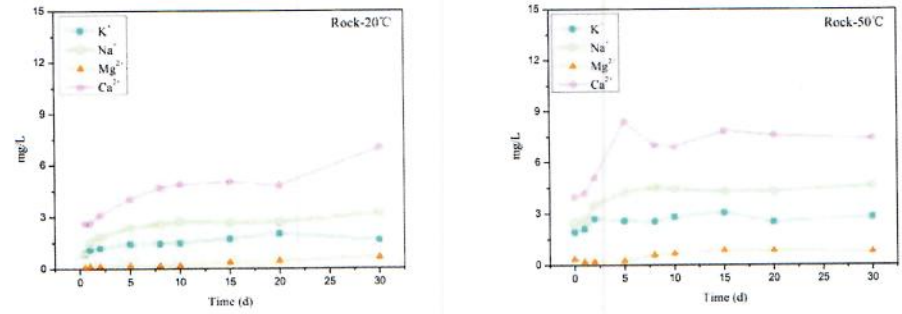


Figure 5. Variation in the content of the main cations in oil shale ash-aqueous solution under different temperature reaction conditions.

The variation in the content of the main cations in the surrounding rock-aqueous solution with different reaction temperatures is shown in Figure 6. With increasing reaction time, the content of cations showed an upwards trend. Under the reaction conditions of 20 °C and 50 °C, the content of Ca^{2+} in the aqueous solution was the highest, followed by Na^{+} and K^{+}, and Mg^{2+} was the lowest. The content of Na^{+} is the highest at 80 °C and 100 °C, followed by Ca^{2+}, K^{+}, and Mg^{2+}. With increasing reaction time, the cationic content in aqueous solution increased steadily under the reaction condition of 80 °C but fluctuated greatly under the reaction condition of 100 °C.



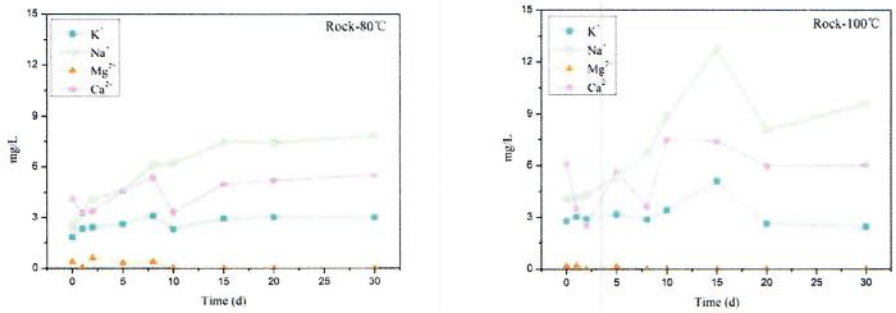


Figure 6. Variation in the content of the main cations in the oil shale surrounding rock-aqueous solution under different temperature reaction conditions.

3.3. *Main anion variation characteristics*

The variation trend of the major anion content in the oil shale-aqueous solution under different temperature reaction conditions is shown in Figure 7. The content of HCO_3^- is always the highest, followed by Cl^-. When the reaction temperature was 20 °C, 50 °C and 80 °C, the content of Cl^- fluctuate; but increased significantly when the reaction temperature was 100 °C. After 30 days of reaction, the content of Cl^- reached 15.4 mg/L. The content change of SO_4^{2-} is similar to the content change of Cl^-, and the change is small at reaction temperatures of 20 °C, 50 °C, and 80 °C, but increases sharply at a reaction temperature of 100 °C. The contents of F^- and NO_3^- in the aqueous solution are always low at different temperature gradients.

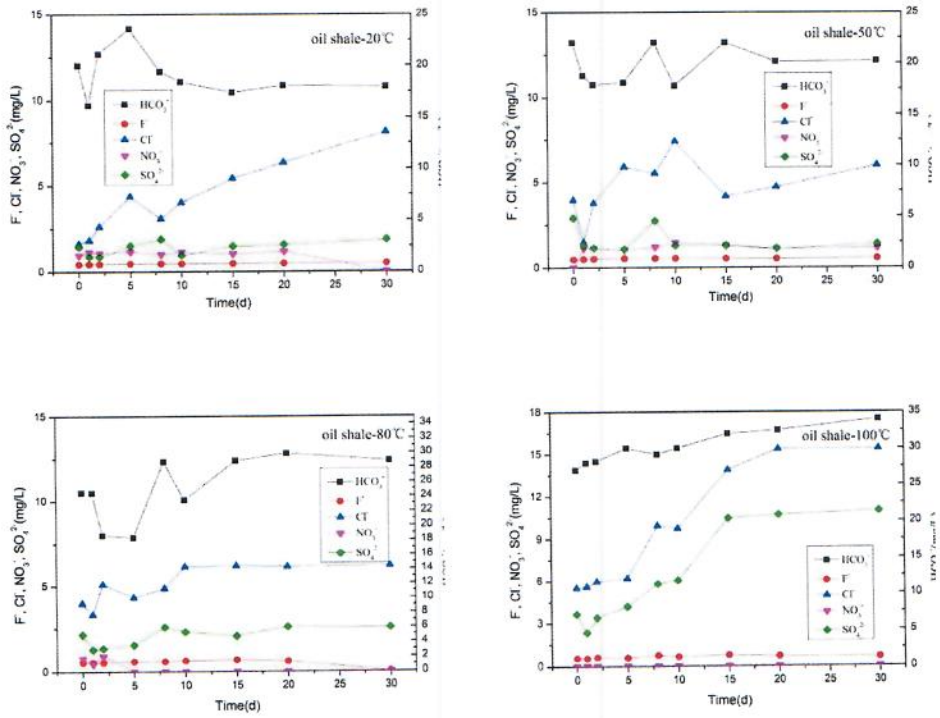


Figure 7. Variation in the content of the main anions in oil shale-aqueous solution under different temperature reaction conditions.

The variation in the main anion content in oil shale ash slag-aqueous solution with reaction temperature is shown in Figure 8. HCO_3^- is the main anion in aqueous solution, the content of HCO_3^- is greater than the content of oil shale aqueous solution, and the content is more than 20 mg/L. The content of HCO_3^- decreases with increasing reaction time in aqueous solutions with higher reaction temperatures (80 °C and 100 °C). Different from oil shale aqueous solution, the content of SO_4^{2-} in aqueous solution increases significantly, and SO_4^{2-} becomes the second-largest anion, surpassing the content of Cl^-. With increasing reaction time, the content of SO_4^{2-} also increases, especially after 30 days of reaction at 80 °C, and the content of SO_4^{2-} in aqueous solution reaches 36.97 mg/L. SO_4^{2-} in aqueous solution generally comes from the dissolution of minerals containing gypsum or other sulfates. In addition, oil shale and its surrounding rock contain a large amount of pyrite. Oxidation of pyrite results in the presence of water-insoluble sulfur in water as SO_4^{2-}. At 100 °C water temperature, the growth rule of Cl^- is similar to that of SO_4^{2-}. The F^- and NO_3^- content is still low, and the NO_3^- content is almost zero.

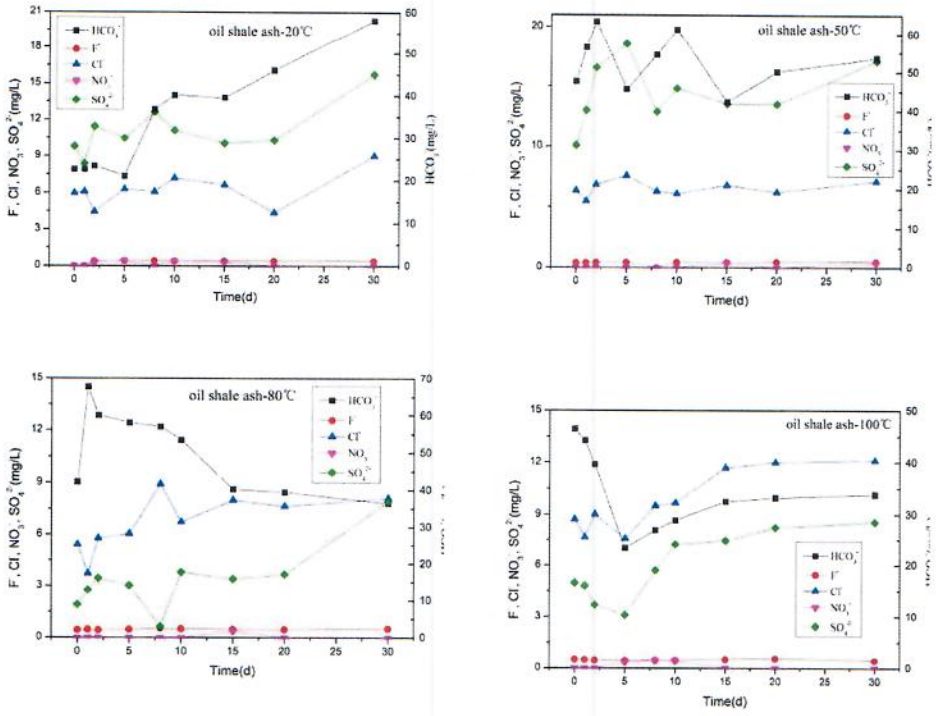


Figure 8. Variation in the content of the main anions in oil shale ash-aqueous solution under different temperature reaction conditions.

Figure 9 describes the changes in the main anion content in the surrounding rock-aqueous solution at different reaction temperatures. Under the reaction conditions of 20 °C, 50 °C, and 80 °C, the variation trend of the main anions in the oil shale surrounding rock water solution is similar to the variation trend of the main anions in the oil shale water solution. HCO_3^- is the main anion, followed by Cl^-, and the content of HCO_3^- and Cl^- gradually increases with time. However, at the reaction temperature of 100 °C, HCO_3^- and Cl^- content changes differently from other temperature conditions, and both of these ions increase first and then decrease with the reaction time. The content of SO_4^{2-}, F^- and NO_3^- in the aqueous solution did not change significantly and remained at a low level.

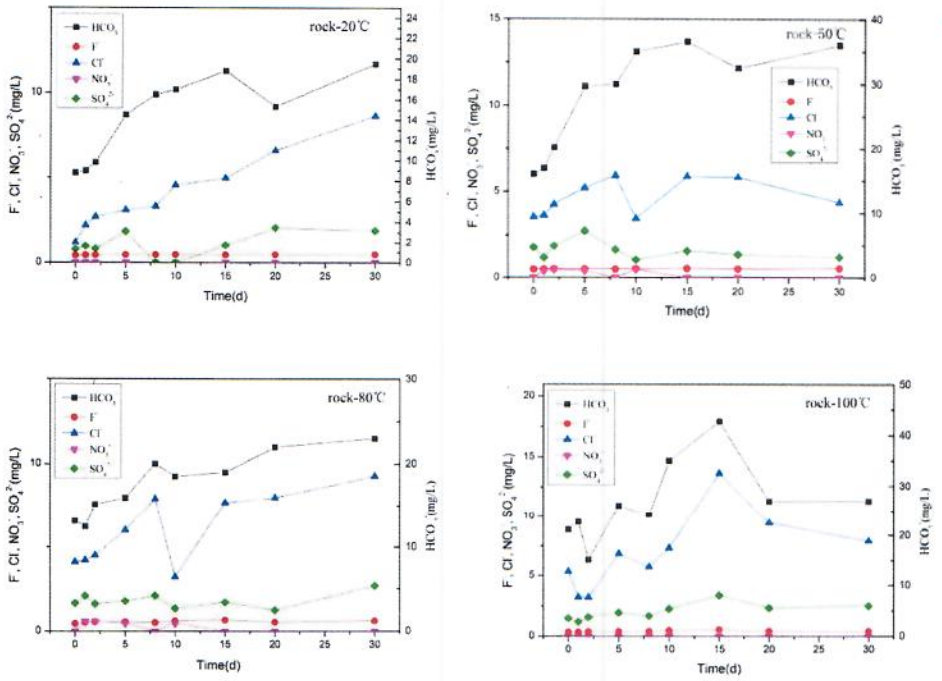


Figure 9. Variation in the content of the main anions in the surrounding rock-aqueous solution under different temperature reaction conditions.

4. Discussion

4.1. Changes in the water chemistry

The Piper diagram can reflect the chemical composition of water–rock interactions in an aqueous solution, as shown by the Piper diagrams for different types of aqueous solutions (Figure 10). As shown in Figure 10-a, in the oil shale-aqueous solution, the dominant cation is Ca^{2+}, the dominant anion is HCO_3^-, and the hydrochemical type is HCO3·Cl-Ca·Na at 20°C and 50°C. At 80°C and 100°C, the dominant cations are Na^+ and K^+, the dominant anions are HCO_3^-, and the hydrochemical types are HCO3-Na·Ca and HCO_3·Cl-Na, respectively. In the oil shale-ash-aqueous solution (Figure 10-b), the dominant cation is Ca^{2+}, the dominant anion is HCO_3^- at 20°C, and the hydrochemical type is HCO_3--Ca·Na. At 50°C, the dominant cations are Ca^{2+}, Na^+ and K^+, the dominant anion is HCO_3^-, and the hydrochemical type is HCO_3-Na +K·Ca. At 80°C and 100°C, the dominant cations are Ca^{2+}, Na^+ and K^+, the dominant anions are HCO_3^- and SO_4^{2-}, and the hydrochemical type is SO_4·HCO_3-Na +K. For the surrounding rock-aqueous solution, Figure 10-c shows that the dominant cation is Ca^{2+}, the dominant anion is HCO_3^- at 20°C, and the hydrochemical type is HCO_3·Cl-Ca·Na. At 50°C, the dominant cations are Ca^{2+}, Na^+ and K^+, the dominant anion is HCO_3^-, and the hydrochemical type is HCO_3-Ca·Na. At 80°C, the dominant cations are Ca^{2+}, Na^+ and K^+. At 100°C, the dominant cations are Na^+ and K^+, the dominant anions are HCO_3^- and SO_4^{2-}, and the hydrochemical types are HCO_3·Cl-Na·Ca.

In Figure 10-d, the grey arrows show that 1) in the three aqueous solutions, the total contents of Ca^{2+} and Ca^{2+}+Mg^{2+} decrease gradually with increasing reaction temperature, indicating that calcite ($CaCO_3$) and dolomite ($CaMg(CO_3)_2$) precipitates from the aqueous solution with increasing temperature. 2) The SO_4^{2-} contents of different aqueous solutions are significantly different. The content of SO_4^{2-} in the oil shale-ash-aqueous solution is the highest, followed by that in the oil shale-aqueous solution, and the content of SO_4^{2-} in the surrounding rock-aqueous solution is the lowest. However, SO_4^{2-} is mainly derived from the oxidation of pyrite (Fe_2S), indicating that a large amount of pyrite (Fe_2S) is released

from oil shale by the in situ pyrolysis of oil shale and exists in groundwater in the form of SO_4^{2-} after interacting with water, which will change the hydrochemical type of the groundwater from its original condition.

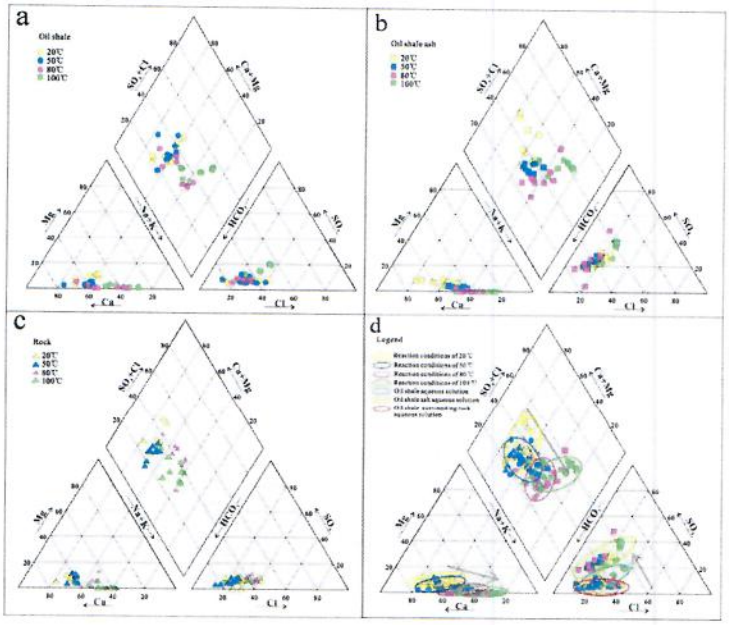


Figure 10. Piper ternary diagrams of water–rock interactions in aqueous solution with different reaction conditions.

4.2. The source of the major components

Factor analysis can determine the hidden representative factors in many variables. The hypothesis of the relationship between variables can be tested by subsuming variables of the same nature into a factor[32-33]. Through SPSS software, general principal component extraction and variance maximum orthogonal rotation factor analysis were used to obtain the results presented in Tables 1-3. The result of the KMO test was 0.553, and the result of Bartlett's test was 1046.244, indicating that factor analysis could be carried out among variables.

Table 1. KMO and Bartlett test result.

Kaiser-Meyer-Olkin test		0.553
Bartlett test result	Approximate chi-square	1046.244
	df	78
	Sig.	0.000

It can be seen from the factor contribution rate (Table 2) that the eigenvalues of the first four factors were greater than 1, and the sum of the eigenvalues of the first four factors accounted for 75.223% of the total eigenvalues, so the first four factors were extracted as the main factors. The following conclusions can be drawn from the factor loading after rotation (Table 3).

Table 2. Total variance explaination.

		Initial eigenvalue	
Common factor	Eigenvalues	Variance contribution rate (%)	Cumulative variance contribution rate (%)
1	4.407	33.903	33.903

2	2.302	17.71	51.613
3	1.682	12.941	64.554
4	1.387	10.669	75.223

Table 3. Rotated factor loading matrix.

Parameter	Factor 1	Factor 2	Factor 3	Factor 4	Commonality
K^+	**0.939**	-0.125	-0.016	-0.054	0.901
Na^+	**0.784**	-0.318	0.456	0.088	0.931
HCO_3^-	**0.884**	0.205	0.073	0.132	0.846
SO_4^{2-}	**0.876**	-0.078	0.023	-0.052	0.777
Temperature	0.293	**-0.784**	0.187	0.223	0.786
Mg^{2+}	-0.106	**0.881**	0.047	0.043	0.791
Ca^{2+}	0.488	**0.66**	0.142	0.215	0.74
Time	0.139	0.209	**0.799**	-0.011	0.701
Cl^-	0.506	-0.279	**0.658**	0.091	0.775
F^-	-0.072	-0.423	**0.527**	-0.262	0.53
Fe^{2+}	-0.127	-0.001	**0.521**	0.49	0.527
Lithology	-0.141	0.123	-0.094	**0.824**	0.723
NO_3^-	-0.354	0.139	-0.063	**-0.776**	0.751

4.3. Formatting

The variance contribution rate of the first principal Factor F1 is 33.903%, which is mainly composed of K^+, Na^+, HCO_3^- and SO_4^{2-}. According to the previous correlation analysis, there is a strong correlation between these four ions, indicating that they may have the same material source or formation process. According to XRD, K^+ in aqueous solution mainly comes from the dissolution of illite ($KAl_2[(SiAl)_4O_{10}]\cdot(OH)_2\cdot nH_2O$):

$$K_{0.5}Mg_{0.25}Al_{2.3}Si_{3.5}O_{10}(OH)_2 + 11/10H^+ + 63/20H_2O \rightarrow 23/20Al_2Si_2O_5 + 1/2K + 1/4Mg^{2+} + 6/5Si(OH)_4 \quad (1)$$

Na^+ comes from the dissolution of plagioclase ($Na[AlSi_3O_8]$-$Ca[Al_2Si_2O_8]$) and montmorillonite ($(Na,Ca)_{0.33}(Al,Mg)_2[Si_4O_{10}](OH)_2\cdot nH_2O$):

$$NaAlSi_3O_8 + H^+ + 9/2H_2O \rightarrow 1/2Al_2Si_2O_5(OH)_4 + Na^+ + Si(OH)_4 \quad (2)$$

$$3Na_{1/3}Al_{7/3}Si_{11/3}O_{10} + 30H_2O + 6OH^- \rightarrow Na^+ + 7Al(OH)_4^- + 10H_4SiO_4 \quad (3)$$

The HCO_3^- comes from the dissolution of dolomite ($CaMg(CO_3)_2$) and calcite ($CaCO_3$):

$$CaCO_3 + CO_2 + H_2O \rightarrow Ca^{2+} + 2HCO_3^- \quad (4)$$

$$CaMg(CO_3)_2 + CO_2 + H_2O \rightarrow Ca^{2+} + Mg^{2+} + 4HCO_3^- \quad (5)$$

SO_4^{2-} comes from the dissolution of gypsum ($CaSO_4\cdot 2H_2O$) or other sulphates and the oxidation of pyrite (FeS_2):

$$2FeS_2 + 7O_2 + 2H_2O \rightarrow 2FeSO_4 + 4H^+ + 2SO_4^{2-} \quad (6)$$

Therefore, F1 reflects the influence of the dissolution of minerals in the sample on the chemical composition of groundwater.

The variance contribution rate of the second main Factor F2 is 17.71%, which is mainly composed of the temperature, Mg^{2+} and Ca^{2+} variables. According to XRD analysis, Ca^{2+} and Mg^{2+} in aqueous solution mainly come from the dissolution of dolomite

($CaMg(CO_3)_2$) and calcite ($CaCO_3$). Therefore, F2 indicates that temperature has a great influence on the dissolution of this kind of mineral. However, HCO_3^- does not belong to the same factor as Mg^{2+} and Ca^{2+}, indicating that HCO_3^- may have other sources. The proportion coefficient can be used to analyse the origin and evolution characteristics of hydrochemical components, and the molar ratio of different ions can be used to describe the hydrochemical characteristics of different groundwater masses to further identify the lithology and origin of the components flowing through the aquifer. In general, if Ca^{2+}, Mg^{2+}, and HCO_3^- in water are mostly derived from carbonate minerals, then the ratio of (Ca^{2+}+Mg^{2+}) to HCO_3^- should theoretically be equal to 1[36]. Figure 12 depicts the ion ratio relationship between Ca^{2+}, Mg^{2+} and HCO_3^-. The results show that in water–rock interaction solution, at a reaction temperature of 20 °C , only some of the samples (Ca^{2+}+Mg^{2+})/HCO_3^- range from 1:1 to 1:2, and most of the sample points are below 1:2, indicating that the dissolution of dolomite ($CaMg(CO_3)_2$) and calcite ($CaCO_3$) is only part of the source of HCO_3^-. Therefore, the solubility of Na_2CO_3 should take into consideration. When the concentration of Na^+ in an aqueous solution is high, the content of HCO_3^- will exceed the upper limit as related to Ca^{2+}.

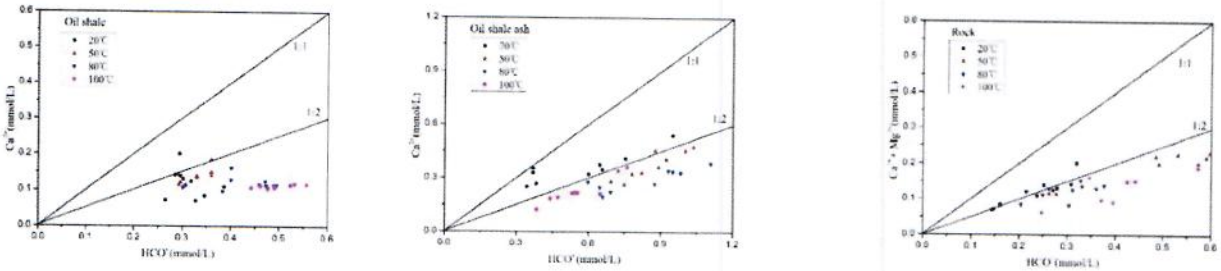


Figure 12. The ratio of Ca^{2+}, Mg^{2+}, and HCO_3^- in aqueous solution under different reaction conditions.

The variance contribution rate of the third principal Factor F3 was 12.941%, which mainly consisted of the reaction time, Cl^-, F^- and Fe^{2+} variables. In these aqueous solutions, Cl^- mainly comes from the dissolution of rock salt (NaCl) or other chlorides ($MgCl_2$, $CaCl_2$). Figure 13 is the scatter plot showing the γNa/γCl ratios in aqueous solution under different reaction conditions. The results show that the content of Na^+ in the solution was higher than that of Cl- (the ratio of Na^+/Cl^- is mostly below the 1:1 line) indicating that rock salt was not the only source of sodium ions in the solution.

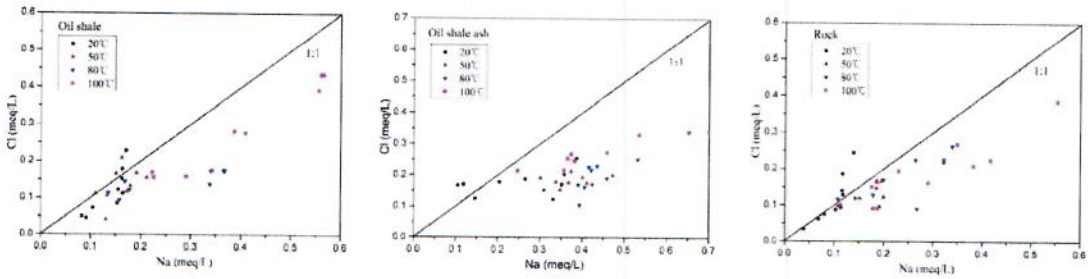


Figure 13. Scatter diagram of γNa/γCl in aqueous solution under different reaction conditions.

According to the XRD results, there is a large amount of pyrite (FeS_2) in both oil shale and the surrounding rock, which is the main source of iron in the aqueous solutions. F^- is mainly derived from the hydrolysis of fluorinated minerals such as fluorite (CaF_2) and apatite ($Ca_5(Cl,F,OH)(PO_4)_3$). Therefore, F3 indicates that the length of the reaction time has great influence on the dissolution of such minerals.

The variance contribution rate of the fourth main Factor F4 is 10.669%, which is mainly composed of the lithology and NO_3^- variables. The content of NO_3^- in aqueous solution is very low and comes mainly from the degradation of nitrogenous organic matter. Oil shale is a kind of mineral rich in organic matter. The heating and retorting process of oil shale is also the process of extracting organic matter from oil shale, so it will cause the differences in organic matter content among the samples. Therefore, F4 indicates that the organic matter content in different rock types varies greatly.

5. Conclusions

A series of experiments on water-rock interaction were conducted to realize the influence of oil shale on groundwater environment during in-situ exploitation. Further, in order to identified the main factors affecting the variation of groundwater, the mineral composition in oil shale and surrounding rock were tested, and accompanied by a statistical analysis of the experiments' results. Based on the results of the work, the following conclusions were drawn:

(1) With the increase of temperature and reaction time, the content of ions in the three aqueous solutions increased. The Ca^{2+} content in the aqueous solution was the highest under the 20 °C and 50 °C temperature conditions, and Na^+ became the principal cation at 80 °C and 100 °C. HCO_3^- is always the main anion in aqueous solution under different reaction conditions.

(2) Under different reaction conditions, the ion content in oil shale ash - aqueous solution changes the most. The water quality of oil shale ash-aqueous solution is changed into sulfuric acid type at 80 °C and 100 °C. This indicates that pyrolytic oil shale is more likely to participate in the reaction when it comes into contact with water. Attentions should be paid to the isolation of reservoir and aquifer after oil shale in-situ exploitation.

(3) The source of the main components in the aqueous solution was identified by factor analysis. The results showed that the mineral type had the greatest influence on the ionic components, followed by temperature, reaction time and organic matter content in the rocks.

In short, oil shale in-situ exploitation will affects the inorganic environment of adjacent aquifers. And because of the geological environments of oil shale areas are different, the compositions of oil shale and its surrounding rocks are also different, so the impacts of in-situ mining on groundwater inorganic minerals should be taken into consideration when evaluating in-situ exploitation projects of oil shale.

Author Contributions: Conceptualization, Shuya Hu; writing and editing, Qingyu Li; methodology, Laijun Lu; analysis, Qingyu Li and Shuya Hu; supervision, Quansheng Zhao; project administration, Shuya Hu. All authors have read and agreed to the published version of the manuscript.

Funding: This research was funded by the National Natural Science Foundation "Study on the mechanism of BTEX release and aquifer pollution during in-situ exploitation of oil shale" of China (Grant No. 42002260).

Data Availability Statement: Not applicable.

Acknowledgments: The author acknowledge the support of The National Natural Science Funds of China (42002260).

Conflicts of Interest: The authors declare no conflict of interest.

References

1. Yang, Q., Zhang, X., Xu, S., Wang, Z., Guo, W. (2022) Low-temperature co-current oxidizing pyrolysis of oil shale: Study on the physicochemical properties, reactivity and exothermic characters of semi-coke as heat generation donor. Journal of Petroleum Science and Engineering. 216, 110726. https://doi.org/10.1016/j.petrol.2022.110726
2. Yang, H., Duan, Y. (2014) A feasibility study on in-situ heating of oil shale with injection fluid in China. J. Petrol. Sci. Eng. 122, 304–317. https://doi.org/10.1016/j.petrol.2014.07.025

3. Roehner, R., Panja, P., Deo, M. (2016) Reducing gas flaring in oil production from shales. Energy Fuel. 30 (9), 7524–7531. https://doi.org/10.1021/acs.energyfuels.6b01126
4. Zhang P, Lu S, Li J, Zhang J, Xue H, Chen C. (2017) Comparisons of SEM, Low-Field NMR, and Mercury Intrusion Capillary Pressure in Characterization of the Pore Size Distribution of Lacustrine Shale: A Case Study on the Dongying Depression, Bohai Bay Basin, China. Energy & Fuels 31(9), 9232-9239. https://doi.org/10.1021/acs.energyfuels.7b01625
5. Hu S, Xiao C, Jiang X, Liang X. (2018) Potential Impact of In-Situ Oil Shale Exploitation on Aquifer System. Water 10(5), 649. https://doi.org/10.3390/w10050649
6. Jaber JO, Probert SD. (1999) Environmental-impact assessment for the proposed oil-shale integrated tri-generation plant [J]. Applied Energy, 62(3):169-209. https://doi.org/10.1016/s0306-2619(99)00006-9
7. Taciuk W. (2013) Does oil shale have a significant future? Oil Shale 30 1–5. https://doi.org/10.3176/oil.2013.1.01
8. Wang S, Jiang X, Han X, Tong J. (2012) Investigation of Chinese oil shale resources comprehensive utilization performance. Energy 42(1), 224-232. https://doi.org/10.1016/j.energy.2012.03.066
9. Jiang X, Han X, Cui Z. (2007) New technology for the comprehensive utilization of Chinese oil shale resources. Energy 32(5), 772-777. https://doi.org/10.1016/j.energy.2006.05.001
10. Han X, Niu M, Jiang X. (2014) Combined fluidized bed retorting and circulating fluidized bed combustion system of oil shale: 2. Energy and economic analysis. Energy 74, 788-794. https://doi.org/10.1016/j.energy.2014.07.050
11. Gross SA, Avens HJ, Banducci AM, Sahmel J, Panko JM, Tvermoes BE. (2013) Analysis of BTEX groundwater concentrations from surface spills associated with hydraulic fracturing operations. J Air Waste Manag Assoc 63(4), 424-432. https://doi.org/10.1080/10962247.2012.759166
12. Arthur MA, Cole DR. (2014) Unconventional Hydrocarbon Resources: Prospects and Problems. Elements 10(4), 257-264. https://doi.org/10.2113/gselements.10.4.257
13. Jefimova J, Irha N, Reinik J, Kirso U, Steinnes E. (2014) Leaching of polycyclic aromatic hydrocarbons from oil shale processing waste deposit: a long-term field study. Sci Total Environ 481, 605-610. https://doi.org/10.1016/j.scitotenv.2014.02.105 (2014)
14. Jefimova J, Kirso U, Urb G, Steinnes E, Reinik J, Irha N. (2013) Leachability of Trace Elements from the Aged and Fresh Spent Shale Deposit – a Field Study. Oil Shale 30(3), 456. https://doi.org/10.3176/oil.2013.3.06 (2013)
15. Pan Y, Zhang XM, Liu SH, Yang SC, Ren N. (2012) A review on technologies for oil shale surface retort. Chem Soc Pak 34 (6)1331–1338.
16. Qian JL, Yin L. (2011) Oil Shale-supplementary Energy of Petroleum, 1st ed., Beijing: China Petrochemical Press, Chinese.
17. Gavrilova O, Vilu R, Vallner L. (2010) A life cycle environmental impact assessment of oil shale produced and consumed in Estonia. Resources, Conservation and Recycling 55(2), 232-245. https://doi.org/10.1016/j.resconrec.2010.09.013
18. Velts O, Uibu M, Rudjak I, Kallas J, Kuusik R. (2009) Utilization of oil shale ash to prepare PCC: Leachibility dynamics and equilibrium in the ash-water system. Energy Procedia 1(1), 4843-4850. https://doi.org/10.1016/j.egypro.2009.02.312
19. Trikkel A, Kuusik R, Martins A, Pihu T, Stencel J.M. (2008) Utilization of Estonian oil shale semicoke. Fuel Processing Technology 89(8), 756-763. https://doi.org/10.1016/j.fuproc.2008.01.010
20. Yu F, Sun P, Zhao K.a, Ma L, Tian X. (2020) Experimental constraints on the evolution of organic matter in oil shales during heating: Implications for enhanced in situ oil recovery from oil shales. Fuel 261, 116412. https://doi.org/10.1016/j.fuel.2019.116412
21. Hu S, Wu H, Liang X, Xiao C, Zhao Q, Cao Y, Han X. (2022) A preliminary study on the eco-environmental geological issue of in-situ oil shale mining by a physical model. Chemosphere 287(Pt 1), 131987. https://doi.org/10.1016/j.chemosphere.2021.131987
22. Hu S, Xiao C, Liang X, Cao Y, Wang, X, Li M. (2019) The influence of oil shale in situ mining on groundwater environment: A water-rock interaction study. Chemosphere 228, 384-389. https://doi.org/10.1016/j.chemosphere.2019.04.142
23. Brandt AR. (2008) Converting oil shale to liquid fuels: energy inputs and greenhouse gas emissions of the shell in situ conversion process. Environmental Science & Technology, 42(19), 7489-7495. https://doi.org/10.1021/es800531f
24. Hu S, Xiao C, Liang X, Cao Y. (2020). Influence of water-rock interaction on the pH and heavy metals content of groundwater during in-situ oil shale exploitation. Oil Shale, 37(2), 104. https://doi.org/10.3176/oil.2020.2.02
25. Amy GL. (1978) Contamination of groundwater by organic pollutants leached from in-situ spent shale[J]. Office of Scientific & Technical Information Technical Reports, 3. https://doi.org/10.2172/1064003
26. Wang H, Zhang W, Qiu S, Liang X. (2021) Release characteristics of Pb and BETX from in situ oil shale transformation on groundwater environment. Sci Rep 11(1), 16166. https://doi.org/10.1038/s41598-021-95509-2
27. Erg K. (2006) Changes in groundwater sulphate content in estonian oil shale mining area. Oil Shale, 22(3), 275-289.
28. Arthur MA, Cole DR. (2014) Unconventional Hydrocarbon Resources: Prospects and Problems. Elements 10(4), 257-264. https://doi.org/10.2113/gselements.10.4.257
29. Perens R, Punning J M, Reinsalu E. (2006) Water problems connected with oil shale mining in North-East Estonia [J]. Oil Shale 23(3):228-235.

30. Liu Z, Yang D, Hu Y, Shao J. Low temperature nitrogen adsorption analysis of pore structure evolution in in-situ pyrolysis of oil shale [J]. Journal of Xi'an University of Science and Technology, 2018(38):738-741.
31. Gao Y, Li X, Hua X. Analysis of Groundwater Chemical Characteristics in Red Bed of Chengdu Based on SPSS [J]. Pearl River, 2016, 37(2):36-42.
32. Yang R, Zhou J, Wei X, et al. Hydrochemical characteristics and evolution of groundwater in the eastern plain of Hotian Prefecture, Xinjiang[J]. Environmental Chemistry, 2022, 41(4): 1367-1379.
33. Zhang F, Jin Z, Yu J , et al. Hydrogeochemical processes between surface and groundwaters on the northeastern Chinese Loess Plateau: Implications for water chemistry and environmental evolutions in semi-arid regions[J]. Journal of Geochemical Exploration, 2015(159):115-128. https://doi.org/10.1016/j.gexplo.2015.08.010